

A seismological method for estimating the long-period transition period T_L in the seismic building code

Earthquake Spectra

1–21

© The Author(s) 2023


Article reuse guidelines:

sagepub.com/journals-permissions

DOI: 10.1177/87552930231153673

journals.sagepub.com/home/eqs



Christie Assadollahi, S.EERI¹,
Shahram Pezeshk, M.EERI¹ , and
Kenneth Campbell, M.EERI²

Abstract

Many changes have been made to the design response spectrum used in the ASCE 7 Standard in recent years. One parameter that has not been investigated or revisited since its first appearance in FEMA 450-1/2003 is the long-period transition period parameter, T_L . The long-period transition period parameter was introduced and defined as the corner period that marks the transition from the constant velocity to the constant displacement segments of the design response spectrum. The long-period transition period parameter is primarily important for long-period structures such as high-rise buildings and bridges. The most current estimation of T_L used in engineering design standards is loosely based on a correlation between modal magnitude M_w and T_L that does not account for stress drop $\Delta\sigma$ or the crustal velocity in the source region β . This study aims to include both $\Delta\sigma$ and β in its estimation of T_L . Modal magnitude is obtained from disaggregation data from the 2018 National Seismic Hazard Model (NSHM) for the conterminous United States (CONUS) and from the 2021 NSHM for Hawaii (HI). The parameter β is determined from previous literature. Then, inversion of ground motion models for Central and Eastern United States (CEUS) is used to determine $\Delta\sigma$ for CEUS events, and published information is used to determine $\Delta\sigma$ for Western United States (WUS) events and HI events. Then, the definition of the corner period is used to determine T_L . The results yield a generally more conservative (or longer) estimation of T_L than the estimation that is currently used in engineering design standards.

Keywords

Long-period parameter, building code, seismological parameters, improved seismic design response spectrum, building code response spectrum, TL parameter

Date received: 1 March 2022; accepted: 11 January 2023

¹The University of Memphis, Memphis, TN, USA

²Kenneth W. Campbell Consulting LLC, Beaverton, OR, USA

Corresponding author:

Shahram Pezeshk, Engineering Science Building-Room 104A, The University of Memphis, Memphis, TN 38152, USA.
Email: speszshk@memphis.edu

Introduction

A design response spectrum is used to determine the expected spectral acceleration of structures with different structural periods. For any earthquake, the response spectrum can be highly irregular. However, the idealized Newmark and Hall (1973) design response spectrum has three constant segments: spectral acceleration, spectral velocity, and spectral displacement. The T_L parameter marks the transition between the constant spectral velocity and the constant spectral displacement segments of the response spectrum. The results of this study estimate the long-period transition period parameter T_L . The T_L parameter is the natural period (in seconds) where the spectral acceleration S_a (g) decreases at a faster rate for $T > T_L$.

According to Bommer et al. (2000), the T_L parameter was sometimes considered and was sometimes ignored when constructing response spectra to be conservative. Before its inclusion in US model building codes and design standards, T_L was estimated to be 4 s (USNRC, 1973). However, Crouse et al. (2006) reported that a period of 4 s was too low. T_L was first introduced to the US model building code and design standards in FEMA 450-1: National Earthquake Hazard Reduction Program (NEHRP) Recommended Provisions for Seismic Regulations for New Buildings and Other Structures Provisions (hereafter called “FEMA 450-1”) (Building Seismic Safety Council (BSSC), 2004a). According to Crouse et al. (2006) and FEMA 450-2, T_L can be approximated using the corner period on the Fourier spectrum T_c as:

$$T_L = T_{L(NEHRP)} \approx T_c \approx 10^{-1.25 + 0.3M_w} \quad (1)$$

$T_{L(NEHRP)}$ is the T_L parameter calculated from Equation 1 and used in FEMA 450-1, T_c is the corner frequency of the Fourier amplitude spectrum, and M_w is the modal moment magnitude obtained from a probabilistic seismic hazard analysis (PSHA) disaggregation of 2% probability of exceedance in 50 years hazard (return period of 2475 years) for spectral acceleration at the spectral period of 2 s for the conterminous United States (CONUS) and spectral period of 1 s for Hawaii (HI) (BSSC, 2004b). Equation 1 was introduced in FEMA 450-1 and FEMA 450-2 and was used to develop the national map of the T_L parameter in the ASCE 7 Standard (American Society of Civil Engineers (ASCE), 2005; BSSC, 2004a, 2004b). Crouse et al. (2006) state that Equation 1 is based on the seismic source model of Brune (1970); however, there is no calculable relationship between Brune’s seismic source theory and Equation 1. Equation 1 does not account for the stress drop $\Delta\sigma$ or the crustal velocity of the source region β (hereafter called “source velocity”), whereas the Brune’s seismic source model does. The determination of T_L has not been revisited or studied since its introduction. A formulation that includes regional seismological parameters would allow for a more customized estimation of T_L based on the geographic location.

Further simplification was applied to Equation 1 to smooth T_L map boundaries by providing a single estimate for various magnitudes. Figure 1 compares Equation 1 $T_{L(NEHRP)}$ and the simplification used in the ASCE 7 Standard to develop $T_{L(NEHRP)sim}$ contour maps (BSSC, 2004b). The simplification is meant to help smooth boundaries for the ASCE 7 Standard maps. However, the simplification is generally not conservative when compared to Equation 1. Underestimating T_L is not conservative because it causes the spectral acceleration to decrease prematurely with respect to the natural period of the structure.

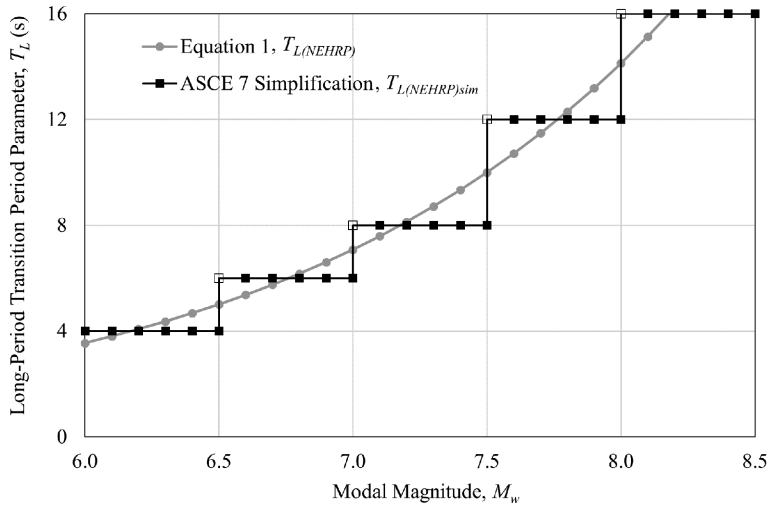


Figure 1. Comparison of Equation 1, $T_{L(NEHRP)}$ and simplification used in the ASCE 7 standard, $T_{L(NEHRP)sim}$ (ASCE, 2005; BSSC, 2004b).

Figure 2 shows the ASCE 7 Standard existing maps for T_L for the CONUS and HI (ASCE, 2005, 2016). The maps shown in Figure 2 were developed using the simplification shown in Figure 1.

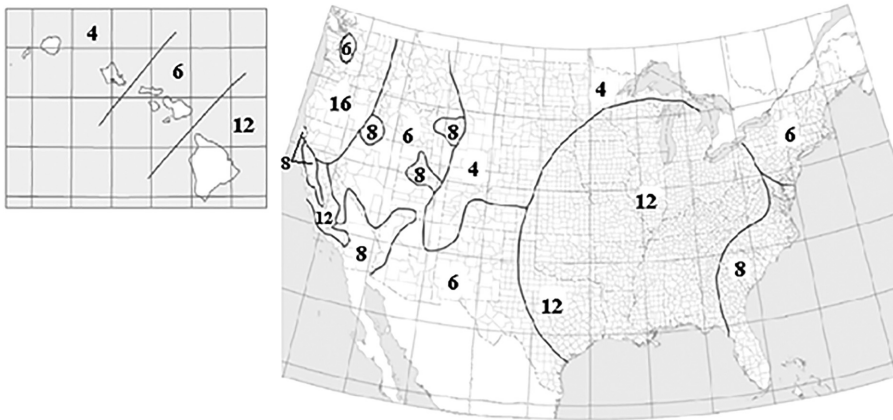


Figure 2. Mapped long-period transition period, T_L (s) for the CONUS (Figure 22-14 of BSSC, 2015) and Hawaii (Figure 22-16 of BSSC, 2015). The bold numbers in each region represent T_L for that region.

Changes to the design response spectrum in the US building codes

Figure 3 shows the design response spectrum presented in FEMA 450-1 with T_L in bold; this is the first design response spectrum to include T_L in a US model building code (BSSC, 2004a). The two-period design response spectrum shown in Figure 3 was the preferred

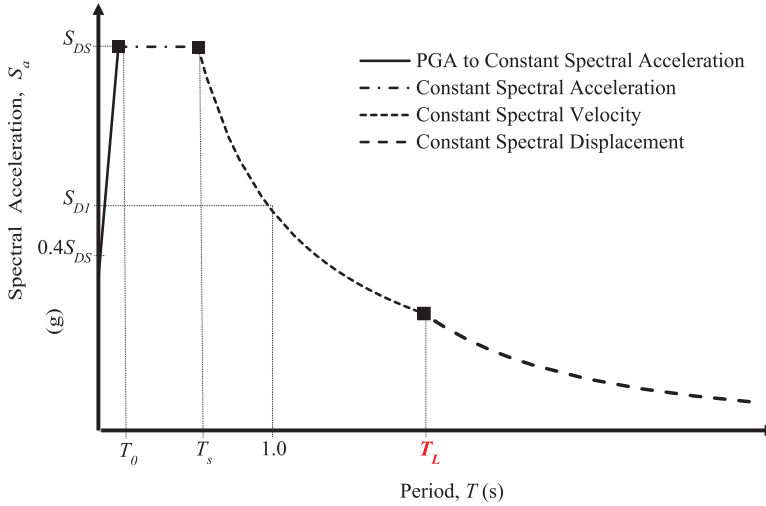


Figure 3. Generic two-period response spectrum, first presented in FEMA 450-1 (BSSC, 2004a).

design response spectrum used by the ASCE 7-05 Standard until the introduction of the multi-period response spectrum (MPRS) in the 2020 Edition of FEMA 450-1 and ASCE 7-22 (ASCE, 2022; BSSC, 2020). In MPRS, the shape of the response spectrum no longer adheres strictly to constant acceleration, constant velocity, and constant displacement segments shown in Figure 3. The MPRS only approximately contains these three segments with smooth and continuous transitions in between.

T_L is an important parameter in the two-period design response spectrum, because it affects both the constant spectral velocity and constant spectral displacement branches. While the two-period design response spectrum shown in Figure 3 is no longer the preferred criteria in the design requirements for FEMA 450-1, the parameter T_L is still a pertinent parameter and is still calculated using the simplification of Equation 1 (BSSC, 2020).

Kircher & Associates (2015), in their critique of the ASCE 7-16 Standard, introduced the need for MPRS, particularly for the underestimation of ground motions at soft-soil sites (D and E). The short-term solution to address this issue was to require site-specific procedures for soft-soil sites to determine S_1 (1 s spectral acceleration at the NEHRP B/C site condition) or S_S (0.2 s spectral acceleration at the NEHRP B/C site condition) if they exceed certain levels. The USGS 2018 update of the US National Seismic Hazard Model (NSHM) expanded the number of periods from just 2 to 22 to accommodate the development of an MPRS as well as the traditional two-period response spectrum (Petersen et al., 2019). There are eight soil site classes (the original NEHRP site classes and the boundary site classes B/C, C/D, and D/E). The introduction of the MPRS in FEMA 450-1 did not include changes to the determination of T_L ; however, the use and the function of T_L in the construction of the response spectrum is different (BSSC, 2020; Kircher et al., 2019).

The MPRS is the preferred response spectrum with two exceptions: a site-specific ground motion analysis is performed, or the MPRS is not available for the site. If the MPRS is not available for the site, then the two-period design response spectrum shown in Figure 3 is used. The following block of text is a direct quote from Section 11.4.5.1 of ASCE 7-22 describing the development of the MPRS:

1. At discrete values of period, T , equal to 0.0, 0.01, 0.02, 0.03, 0.05, 0.075, 0.1, 0.15, 0.2, 0.25, 0.3, 0.4, 0.5, 0.75, 1.0, 1.5, 2.0, 3.0, 4.0, 5.0, 7.5, and 10 s, the 5%-damped design spectral response acceleration parameter, S_a , shall be taken as 2/3 of the multi-period 5%-damped MCE_R response spectrum from the USGS Seismic Design Geodatabase for the applicable site class.
2. At each response period, T , less than 10 s and not equal to one of the discrete values of period, T , listed in item 1 above, S_a , shall be determined by linear interpolation between values of S_a , of item 1 above.
3. At each response period, T , greater than 10 s, S_a , shall be taken as the value of S_a at the period of 10 s of item 1 above, factored by $10/T$, where the value of T is less than or equal to that of the long-period transition period, T_L , and shall be taken as the value of S_a at the period of 10 s, factored by $10T_L/T^2$, where the value of T is greater than that of the long-period transition period, T_L .

The authors noted that the procedure for the MPRS results in a discontinuity in the response spectrum when T_L is less than 10 s; the discontinuity occurs between the S_a at 10 s, S_{a10} , and at a period greater than 10 s.

The authors recommend that the Item 3 of the Section 11.4.5.1 of ASCE 7-22 be corrected. Currently, Item 3 explains how to calculate the 5%-damped design spectral response acceleration parameter, S_a , when the period of interest T is greater than 10 s. Item 3 can be summarized using:

$$S_a = \frac{(10)S_{a10}}{T} \quad (2a)$$

when the period of interest T is less than T_L , and S_{a10} is the spectral acceleration at a period of 10 s, and:

$$S_a = \frac{(10)T_LS_{a10}}{T^2} \quad (2b)$$

when the period of interest T is greater than T_L . An issue arises when the period of interest is greater than 10 s and T_L is less than 10 s. Then, immediately after 10 s, the S_a would be calculated using Equation 2b. If T_L is less than 10 s, the authors propose the following equation for periods of interest greater than 10 s:

$$S_a = \frac{(10^2)S_{a10}}{T^2} \quad (2c)$$

Equation 2c ensures continuity. Figure 4 shows the MPRS presented in the 2020 Edition of FEMA 450-1 as the default design response spectrum; Figure 4 shows an example in which T_L is greater than 10 s.

Figure 5 shows an example of a generic MPRS with T_L less than 10 s; Figure 5 includes both the current code language Equation 2b and our proposed Equation 2c. The discontinuity using the current code language (Equation 2b) is apparent in Figure 5.

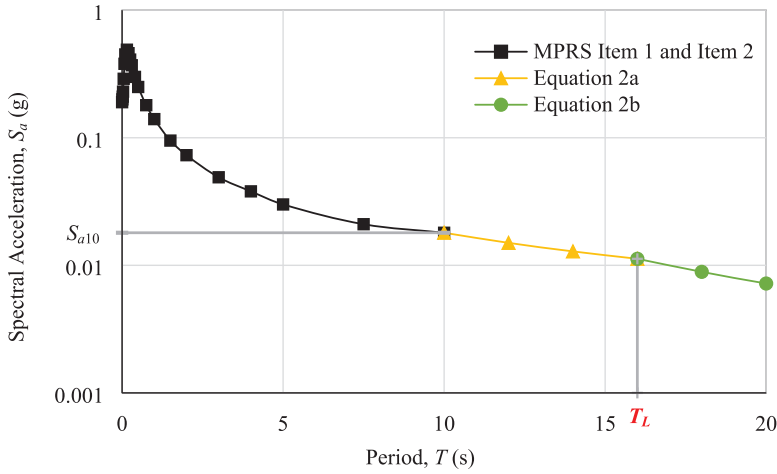


Figure 4. Generic MPRS, first presented in the 2020 edition of FEMA 450-I (BSSC, 2020).

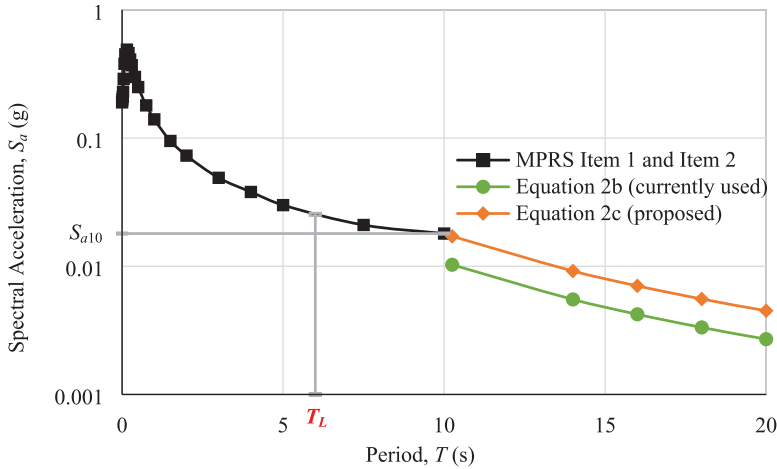


Figure 5. Generic MPRS with T_L less than 10 s and proposed Equation 2c.

Research related to T_L and response spectra

Although T_L has not been directly investigated in the United States, there has been limited research conducted related to determining T_L in other countries. Fauzi et al. (2011) developed a map of T_L in Indonesia based on the methodology proposed by Crouse et al. (2006) and used in FEMA 450-1 (BSSC, 2004a). According to Crouse et al. (2006), the parameter T_L can be approximated by T_c . However, this is an assumption with no proven basis. McVerry et al. (2017) studied the estimation of T_L in New Zealand based on both Brune-type expressions and analyzing response spectra from recent large New Zealand Earthquakes. McVerry et al. (2017) echoed the need for further investigation into the relationship between T_c and T_L .

In the United States, there has been a wide range of research conducted on the construction of smooth response spectra. Malhotra (2006) developed a method of constructing a smooth response spectrum based on peak ground accelerations, peak ground velocity,

and peak ground displacements. Li et al. (2016) built upon the work of Malhotra by considering more ground motions at a variety of soil sites, resulting in the development of site design spectrum coefficients to modify the spectral values of Newmark design spectra in the acceleration-sensitive, velocity-sensitive, and displacement-sensitive regions based on soil site class.

In addition to research related to T_L , research has also been conducted on the disaggregation of seismic hazard into source contributions. Disaggregation of seismic hazard shows the relative contribution of magnitudes and distances contributing to the probability of exceedance of a certain level of hazard. Some sources of literature refer to “deaggregation” instead of “disaggregation,” but both terms refer to the same technique (Bazzurro and Cornell, 1999). Disaggregation techniques have changed over time, as well as disaggregation results from NSHMs (Bazzurro and Cornell, 1999; Harmsen, 2001; Petersen et al., 2019). A disaggregation of seismic hazard was completed specifically for the construction of T_L maps for FEMA 450-1/2003 (Crouse et al., 2006). Disaggregation was again completed by USGS in 2008, 2014, and 2018 for the CONUS and in 2021 for HI for updates to the NSHM. However, T_L has not been re-computed based on changing disaggregation results over the years.

A different approach to estimating T_L

Our objective for this research is to develop an improved estimation of T_L . Instead of calculating T_L only as a function of M_w as in Equation 1, the definition of corner period will be utilized to estimate T_L as:

$$T_L \approx T_c = \frac{1}{f_c} = \frac{1}{4.9(10^6)\beta} \left(\frac{10^{1.5(10.7 + M_w)}}{\Delta\sigma} \right)^{1/3} \quad (3)$$

Equation 3 is the definition of the corner period of the Fourier amplitude spectrum T_c developed by Brune (1970), where the seismic moment M_o is substituted with its definition in terms of M_w developed by Hanks and Kanamori (1979). The corner frequency f_c is the inverse of the corner period, which is also defined as the source duration T_D (Boore, 2003).

There are two primary concerns with using Equation 3: (1) it assumes a single-corner frequency (SCF) spectrum and (2) the relationship between T_c and T_L . Both concerns also exist with the original estimation of T_L in Equation 1.

Atkinson and Silva (2000) stated that the primary issue with using an SCF spectrum is that SCF models consistently overpredict ground motions from moderate and large earthquakes at low and intermediate frequencies (0.1–2 Hz), making an SCF model undesirable. However, double-corner frequency (DCF) models have been developed where the lower corner frequency f_{c1} is defined as proportionally the same as the SCF f_c shown in Equation 3 (Ji and Archuleta, 2021), that is:

$$\frac{1}{f_{c1}} \propto \frac{1}{\beta} \left(\frac{M_o}{\Delta\sigma} \right)^{1/3} \quad (4)$$

So, for the sole purpose of estimating the corner period, an SCF and DCF model yield the same result. Moreover, SCF models are still being developed and used in many ground motion models (GMMs), including the six Boore models presented in the NGA-East

project (Goulet et al., 2015). For these reasons, an SCF model was determined to be appropriate for this application.

FEMA 450-1 considers T_c and T_L approximately equal (BSSC, 2004b). T_L is a parameter that is used to represent a specific period when the displacement spectrum is constant of multiple earthquakes that could occur in a geographic location, rather than an actual specific, measurable quantity. McVerry et al. (2017) studied the estimation of T_L in New Zealand based on both Brune-type expressions and analyzing response spectra from five recent large New Zealand Earthquakes. They concluded that for New Zealand the Brune-type seismological expressions were sufficient to estimate T_L for lower magnitude earthquakes, and the analysis of response spectra better estimated T_L for the larger earthquakes (“larger” meaning earthquakes with $M_w \geq 6$). However, they also stated that further investigation into the relationship between T_c and T_L should be conducted.

Methodology

Following Equation 3, we use regional estimates of M_w , β , and $\Delta\sigma$ to estimate T_L . Estimations of parameters β and $\Delta\sigma$ are split into three broad regions of the United States: the Central and Eastern United States (CEUS) and Western United States (WUS) that comprise the CONUS, and HI. WUS includes all locations in the CONUS west of the boundary used in the 2018 Update of the US NSHM (Petersen et al., 2019). The modal magnitude M_w for a 2% probability of exceedance in 50 years hazard can be determined using the USGS Disaggregation Web Tool of the 2018 NSHM of the CONUS and the 2021 NSHM of HI (Petersen et al., 2019, 2022; USGS, 2022). The details of estimating all parameters are described next.

Estimation of β

We use the well-established estimates of source velocity from previous research: $\beta = 3.7$ km/s for CEUS, $\beta = 3.5$ km/s for WUS, and $\beta = 3.8$ km/s for HI (Wong et al., 2021; Zandieh et al., 2018).

Estimation of $\Delta\sigma$

Zandieh et al. (2018) developed estimates for the stress drop in the WUS using an inversion of five ground motion prediction equations (GMPEs) that were developed as part of the PEER NGA-West2 Project (Bozorgnia et al., 2014). The GMPEs used for the inversion are ASK14 (Abrahamson et al., 2014), BSSA14 (Boore et al., 2014), CB14 (Campbell and Bozorgnia, 2014), CY14 (Chiou and Youngs, 2014), and I14 (Idriss, 2014). We used Zandieh et al.’s (2018) study for WUS sites. Figure 6 shows the estimations of stress drop for the WUS as a function of magnitude.

From Figure 6, the stress drop in WUS ranges from 100 bars to almost 250 bars. A stress drop that rises and then plateaus and/or decreases with magnitude is expected from inversion results (Zandieh et al., 2018).

We used the GMMs developed for the CEUS (Goulet et al., 2015) to perform an inversion to determine stress drop using an approach similar to that used by Zandieh et al. (2018).

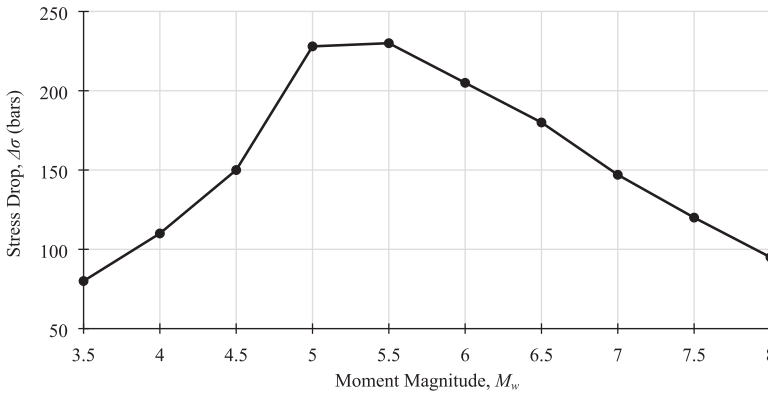


Figure 6. Stress drop estimations for WUS (Zandieh et al., 2018).

For HI, we used an estimate from Wong et al. (2021) of $\Delta\sigma = 20$ bars. Wong et al. (2021) performed an inversion of the 2018–2019 Kalapana sequence recorded by the Hawaiian networks and previously recorded crustal events. Then, they developed a crustal earthquake GMM using the stochastic numerical ground motion modeling approach (Silva et al., 1997). They performed an inversion of Fourier amplitude spectra for stress drops and other seismological parameters for HI.

Inversion

A genetic algorithm (GA) was used to perform the inversion for the stress drop in the CEUS, similar to the GA used to invert for stress drop and other parameters for the WUS sites by Zandieh et al. (2018). Goldberg's GA consists of three basic genetic operators: reproduction, crossover, and mutation. The reproduction operation in the GA is the basic engine of Darwinian natural selection and survival of the fittest (Goldberg, 1989; Koza, 1992). The crossover operation creates variations in the solution population by producing new solution strings that consist of parts taken from selected parent solution strings. The mutation operation introduces random changes in the solution population. In a GA, the mutation operation can be beneficial in reintroducing diversity in a population. In this study, a GA minimized the following objective function:

$$\text{Objective Function} = \sum_{i,j,k} (\log(S_{i,j,k}) - \log(G_{i,j,k}))^2 \quad (5)$$

where $S_{i,j,k}$ is the observed spectral acceleration for magnitude i , distance j , and spectral period k , and $G_{i,j,k}$ is the stochastically predicted value of the spectral acceleration from the inversions.

In any inversion problem, there are trade-offs between parameters. So, each parameter should be constrained within reasonable bounds. The range of each parameter vastly increases or decreases the overall search space for an inversion. A literature review was completed to determine a reasonable search space for the stress drop parameter. Previous estimations of the stress drop in the CEUS have varied greatly. Goulet et al. (2015) summarize the models used in the development of NGA-East GMMs and cite the mean stress drop from one model as low as 50 bars and another as high as 800 bars. Atkinson (1993)

found that CEUS earthquakes have stress drops ranging from 50 to over 400 bars, with a median value of about 150 bars. Boore (2012) determined the stress drop of nine well-recorded earthquakes in the Eastern United States, and the results are also highly varied across the eight earthquakes that the stress drop was estimated for (from 56 bars up to 422 bars). The stress drop was constrained to be between 50 and 600 bars for the inversion, since many estimations of stress drop in the CEUS are within that range.

CEUS ground motion models

The GMMs used for the inversion to estimate the stress drop $\Delta\sigma$ in the CEUS were originally developed by Goulet et al. (2015). Then, Goulet et al. (2018a) developed standard deviation models and a ground motion characterization (GMC) tool to accompany the GMMs. The final report by Goulet et al. (2018a) included 17 GMMs applicable for a range of magnitudes $4 \leq M \leq 8.2$ and distances up to 1500 km. A weighted average of the median spectral acceleration of each of the GMMs we used in the inversion were calculated using the GMC tool developed by Goulet et al. (2018b). For this study, the inversion was performed for 25 periods ranging from 0.01 to 10 s, uniformly distributed in log space, and for 30 values of R_{RUP} ranging from 1 to 300 km, uniformly distributed in log space. The inversion was performed for individual M_w ranging from 4.0 to 8.0 in 0.5 intervals. The V_{s30} value of 3000 m/s was used, with the site condition adjustment of the NGA-East GMM to the B/C site condition ($V_{s30} = 760$ m/s) performed using the site factors in Hashash et al. (2020) and Stewart et al. (2020). Figure 7 shows the estimations for stress drop as a function of moment magnitude.

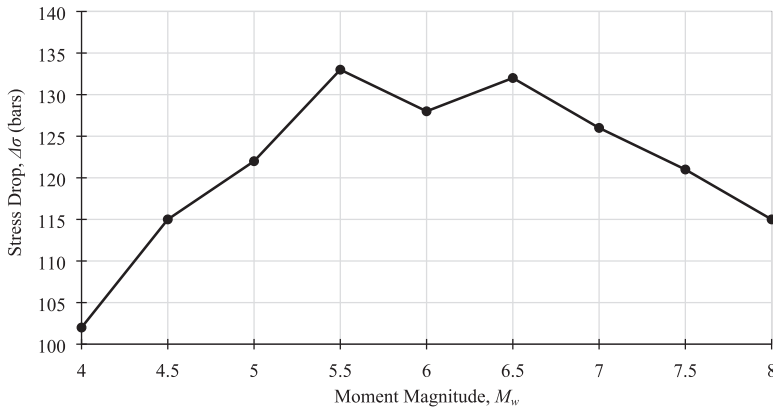


Figure 7. Stress drop estimations for CEUS (this study).

As can be observed from Figure 7, the stress drop in the CEUS has a similar trend to that shown in the WUS; however, the stress drop only varies from 100 to 135 bars, which is very little. The trend shown in Figure 7 is characteristic of stress drop resulting from an inversion.

Determination of M_w

For the CONUS, we obtained the modal magnitude M_w at grid points with a spacing of 0.5°. The M_w is obtained from the USGS Disaggregation Web Tool using a web driver

function of the Selenium module in Python (USGS, 2022). The model used for disaggregation is the NSHM Conterminous US 2018 with a probability of exceedance of 2% in 50 years hazard. In this study, we obtained the modal magnitude M_w disaggregated at a spectral period of 2 and 4 s and compared the results. Recall that in the FEMA 450-1 calculation of T_L , 2 s was the longest spectral period in which disaggregation could be completed. Now, the USGS Disaggregation Web Tool can provide disaggregation results for a spectral period up to 10 s in some regions and 4 s in all regions of the CONUS.

For HI, we developed a grid of points with 0.05° spacing and determined the modal magnitude M_w at each point. The M_w is obtained using the same exact method and tools described for the CONUS. However, the model used for disaggregation is the NSHM Hawaii 2021 and a probability of exceedance of 2% in 50 years hazard (Petersen et al., 2022). For HI, we obtained M_w disaggregated at 1 and 2 s and compared the results. Recall that in the FEMA 450-1 calculation of T_L , 1 s was the longest spectral period in which disaggregation could be completed for HI. Now, the USGS Disaggregation Web Tool can provide disaggregation results for a spectral period up to 10 s in HI.

The hazard level will not change from the disaggregation originally determined to develop T_L maps in FEMA 450-1 and in this study, because the probability of exceedance is the same. A probability of exceedance of 2% in 50 years is used in determining the spectral acceleration for the design response spectrum, so we used the same hazard level for determining M_w in this study.

Comparison of M_w at different spectral periods

When T_L was first developed, a spectral period of 2 s (for the CONUS) and 1 s (for HI) were considered sufficiently long spectral periods to calculate T_L (Crouse et al., 2006). However, in some areas, the modal magnitude at a spectral period of 1 or 2 s can be very different than the modal magnitude at longer spectral periods. So, a sensitivity analysis was conducted. Figure 8a shows a map of the numerical difference between the modal magnitude at 4 s, $M_{w(4s)}$ and modal magnitude 2 s, $M_{w(2s)}$ with all other parameters the same. The spectral period of 4 s was chosen to compare to 2 s, because 4 s is the longest spectral period available at every site in the CONUS. From the estimations of modal magnitude at both spectral periods, we were able to estimate T_L using these different modal magnitudes and compare them. Figure 8b shows the numerical difference between T_L estimated using Equation 3, with the modal magnitude at a spectral period of 4 s, $T_{L(4s)}$ and T_L estimated from the modal magnitude at a spectral period of 2 s, $T_{L(2s)}$.

As can be observed from Figure 8a, the difference between the modal magnitude at spectral periods of 4 and 2 s is less than 1.0 for all the CEUS. However, in the WUS, many areas have a difference of 2, and for a significant area there is a difference of over 3. As can be observed from Figure 8b, again, there is very little variation in the CEUS (except for the New York area), and high variation in the WUS. In the WUS, there is a difference over 5 s in many areas and over 13.5 s difference in a significant area. Further analysis of the correlation between the spectral period and modal magnitude needs to be conducted.

After analyzing Figure 8, we decided to use a spectral period of 2 s for several reasons. First, the estimated T_L from this study at a spectral period of 2 s is already longer (or more conservative) compared to the T_L from FEMA 450-1. Figure 9 shows the mapped modal magnitude at a spectral period of 2 s, used in the calculation of T_L for the CONUS.

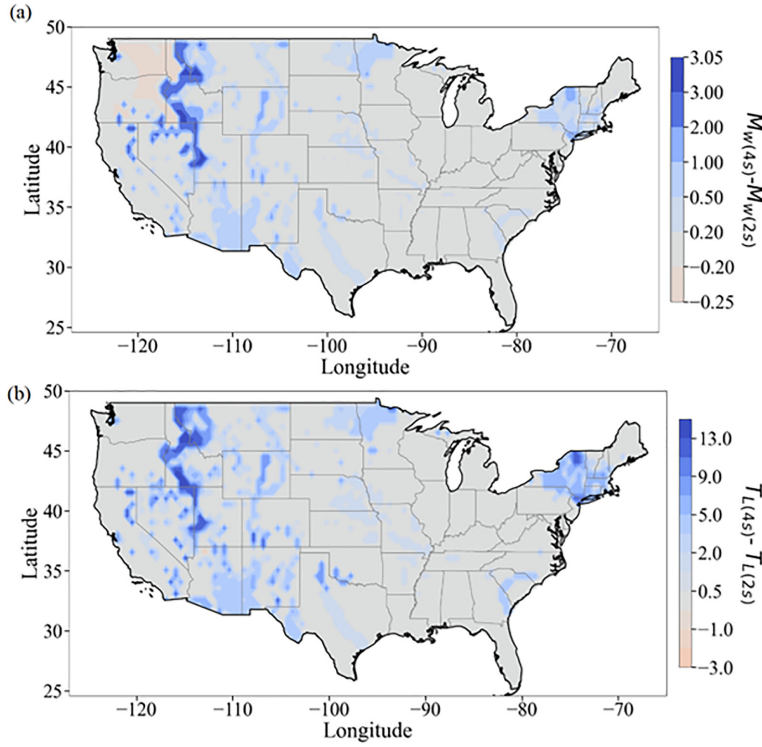


Figure 8. (a) Difference in modal magnitude at spectral period of 4 s, $M_{w(4s)}$ and modal magnitude at spectral period of 2 s, $M_{w(2s)}$. (b) Difference in T_L using Equation 3 with the modal magnitude at a spectral period of 4 s, $T_{L(4s)}$ and T_L using the modal magnitude at a spectral period of 2 s, $T_{L(2s)}$.

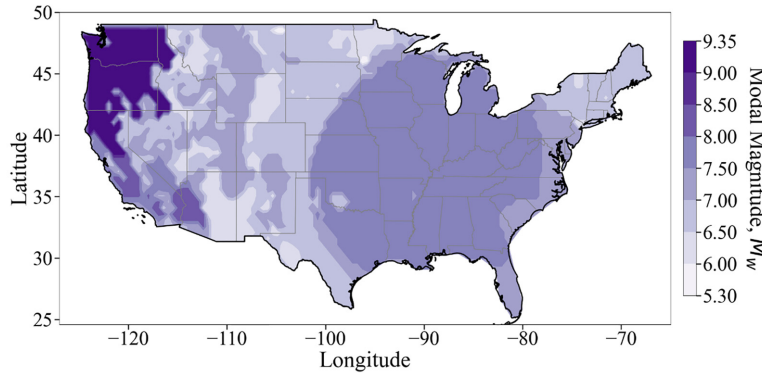


Figure 9. Mapped modal magnitude at a spectral period of 2 s in the CONUS.

As can be observed from Figure 9, the modal magnitude at a spectral period of 2 s ranges from 5.3 to 9.35 in the CONUS. M_w is the largest in the northwest corner of the CONUS and is between 7.5 and 8 in a majority of the CEUS. It should be noted that the M_w disaggregated at a spectral period of 2 s shown in Figure 9 is still different than the M_w disaggregated for the original development of M_w and T_L maps, since

disaggregation has been re-done several times by USGS through the NSHM (Crouse et al., 2006; Petersen et al., 2019).

When T_L was originally developed for HI, M_w was disaggregated at a spectral period of 1 s. Figure 10 shows a map of (a) the numerical difference between the modal magnitude at 2 s, $M_{w(2s)}$ and modal magnitude at 1 s, $M_{w(1s)}$ with all other parameters kept the same for HI and (b) the numerical difference between the modal magnitude at 4 s, $M_{w(4s)}$ and modal magnitude 1 s, $M_{w(1s)}$ with all other parameters kept the same for HI.

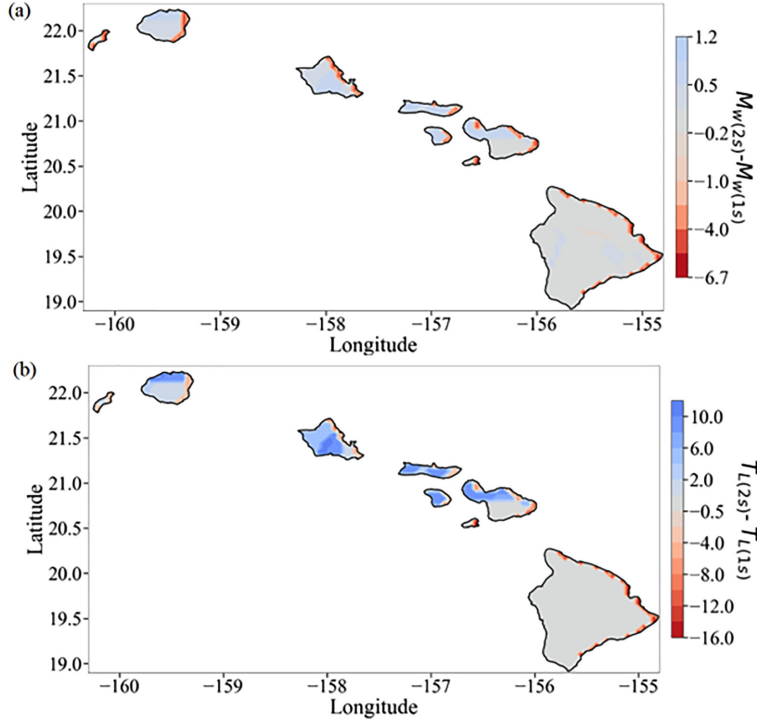


Figure 10. (a) Difference in modal magnitude at spectral period of 2 s, $M_{w(2s)}$ and modal magnitude at spectral period of 1 s, $M_{w(1s)}$ for HI. (b) Difference in T_L using the modal magnitude at a spectral period of 2 s, $T_{L(2s)}$ and T_L using the modal magnitude at a spectral period of 1 s, $T_{L(1s)}$ for HI.

As can be observed from Figure 10a, $M_{w(1s)}$ is much larger than $M_{w(2s)}$ along many of the borders of the islands by as much as 6.7 but are in closer agreement elsewhere. Figure 10a shows conflicting results, as there is no direct correlation between the spectral period and M_w ; a longer spectral period does not always result in a larger M_w . As can be observed from Figure 10b, in some areas, $T_{L(2s)}$ is more than $T_{L(1s)}$ by more than 10 s, and in other areas $T_{L(2s)}$ is almost 16 s less than $T_{L(1s)}$.

After analyzing Figure 10, we recommend using a spectral period of 1 s for HI. The estimated T_L from this study at a spectral period of 1 s is already longer (or more conservative) compared to the simplification of T_L from FEMA 450-1. The differences shown in Figure 10 show a need for further investigation regarding the effect of the spectral period on T_L in HI in future studies. Figure 11 shows the mapped modal magnitude at a spectral period of 1 s, used in the calculation of T_L for HI.

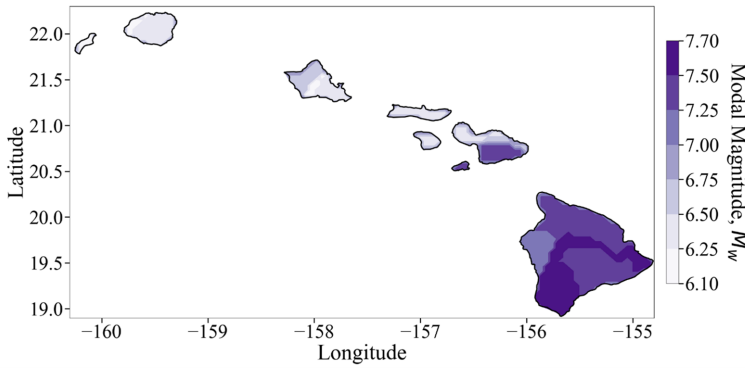


Figure 11. Modal magnitude at a spectral period of 1 s in HI.

In Figure 11, the modal magnitude ranges from 6.1 to 7.7 in HI. It should be noted that the M_w disaggregated at a spectral period of 1 s shown in Figure 11 is still different than the M_w disaggregated for the original development of M_w and T_L maps for HI, since disaggregation has been re-done in HI by USGS through the NSHM (Crouse et al., 2006; Petersen et al., 2022).

The current limit for T_L is 16 s in the WUS and Alaska, citing the analysis of response spectra from simulated ground motions from models of large subduction-zone earthquakes (Crouse et al., 2006; Gregor et al., 2002). However, the response spectra from Gregor et al. (2002) were only developed for a period up to 5 s, making it unclear how that conclusion was made. T_L is currently limited to 12 s in the CEUS, without justification (Crouse et al., 2006). The authors agree that 16 s is a reasonable limit nationally, given that hardly any structures have a fundamental period that high.

Results

Once stress drop was determined as a function of moment magnitude in the WUS and CEUS, and the appropriate modal magnitude was selected, stress drop was mapped corresponding to the estimated modal magnitude at each site. Figure 12 shows the mapped stress drop from the magnitude-dependent estimates from Zandieh et al. (2018) for WUS and the inversion of the GMMs for CEUS completed for this study.

From the regional estimates of stress drop and source velocity, Equation 3 was used to estimate T_L for this study. Figure 13 compares T_L as a function of M_w when using Equation 1, the ASCE 7 simplification of Equation 1, and Equation 3 for the three broad regions of the United States mentioned in this study: CEUS, WUS, and HI.

From Figure 13, FEMA 450-1 has lower values of T_L in the CEUS and WUS for M_w greater than 6.7, whereas FEMA 450-1 has lower values of T_L in HI for M_w greater than 6. The CEUS, WUS, and HI models all estimate a steeper slope for T_L versus M_w than Equation 1 or its simplification. Figure 13 also demonstrates a more customized approach to determining T_L using the methodology in this study; rather than having one line that estimates T_L for the entire United States, this study has three unique lines that estimate T_L in the CEUS, WUS, and HI separately. The slope of the line in Figure 13 is primarily affected by β , whereas the shifting of the line upward and downward is primarily affected by the estimate of $\Delta\sigma$.

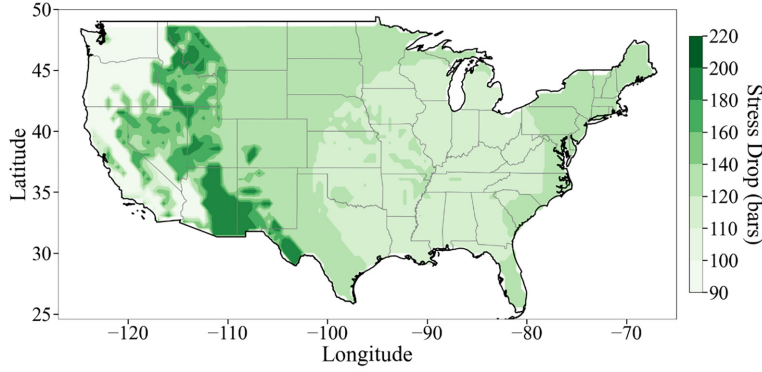


Figure 12. Stress drop (bars) in the CONUS.

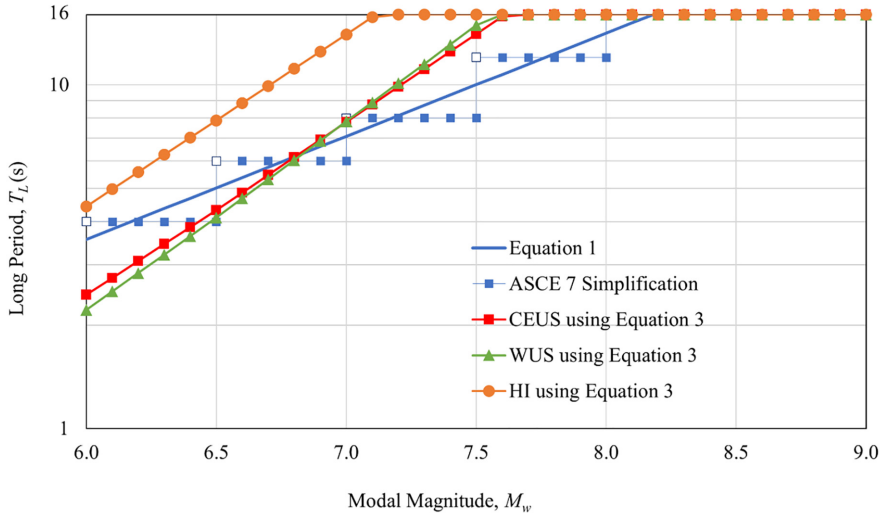


Figure 13. Comparison of T_L used currently (Equation 1; ASCE 7 simplification) and those estimations proposed in this study (CEUS using Equation 3; WUS using Equation 3; HI using Equation 3).

Figure 14 shows estimates of T_L in the CONUS from this study. Figure 15 shows the estimates of T_L in HI from this study. The authors recommend that 16 s is a sufficiently long period to limit T_L nationally, considering that very few structures will have a structural period that long, and that limit is reflected in Figures 14 and 15.

This study's estimates of T_L in Figures 14 and 15 were subtracted from the ASCE 7 simplification of Equation 1, $T_{L(NEHRP)sim}$, to determine the difference (in seconds) between the two at each site. Figure 16 shows the numerical difference between the simplification of FEMA 450-1's Equation 1, $T_{L(NEHRP)sim}$ and T_L estimated from this study in the CONUS. Figure 17 shows the same numerical difference for HI.

Figures 16 and 17 show a significant discrepancy in $T_{L(NEHRP)sim}$ and T_L computed in this study for many regions of the United States. These differences are expected considering that M_w is greater than 5.3 in all locations in the United States and the formulations for T_L developed in this study are longer than $T_{L(NEHRP)sim}$ for $M_w > 6.7$.

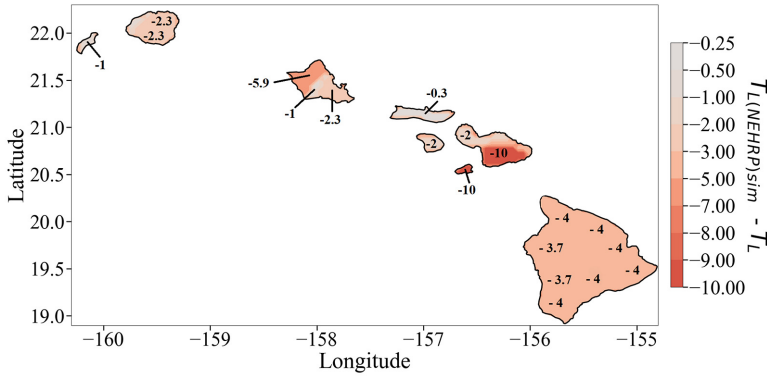


Figure 17. Difference between the ASCE 7 simplification of Equation 1, $T_{L(NEHRP)sim}$ and this study's estimation of T_L in HI. Since all areas of this map are negative, that means that $T_{L(NEHRP)sim}$ is shorter than T_L computed in this study at every location in HI.

It is important to note again that the numerical difference shown in Figures 16 and 17 is between the $T_{L(NEHRP)sim}$ (shown in Figure 1) and Equation 3, not between $T_{L(NEHRP)}$ and Equation 3. The reason why is that it demonstrates the actual change in seconds that T_L could differ in the building codes in the future.

Conclusion

The results of this study are generally more conservative than the estimation of T_L currently used in FEMA 450-1. There are numerous regions where FEMA 450-1's estimation is more conservative; however, it is longer by at most 3 s in those regions, whereas our estimation is longer than FEMA 450-1's estimation by up to 7 s in the CONUS and 10 s in HI.

When T_L was first introduced in Crouse et al. (2006) as a new parameter, it was noted that T_L would likely need to be investigated and refined. However, since its inception, T_L has not been modified. This study aimed to address concerns raised over the estimation of T_L . One concern with the current estimation of T_L is using one equation (ASCE 7 simplification of Equation 1; $T_{L(NEHRP)sim}$) for the entire country, despite differences in seismological parameters. With regional estimations of seismological parameters available, T_L can be calculated anywhere with estimations of $\Delta\sigma$ and β . A concern that was specifically expressed in the introduction of T_L in Crouse et al. (2006) is the harsh borders between areas of a high T_L and an area with a lower T_L . This study estimates T_L on a 0.5° spacing in the CONUS and a 0.05° spacing in HI, resulting in a high-resolution contour map with thin bands between very high values and lower values of T_L . Furthermore, any site within the CONUS is within 17.25 miles of an estimation of T_L , and any site in HI is within 1.725 miles. The last concern raised over the current estimation of T_L is that it has not been updated along with new disaggregation data that has resulted in new estimations of modal magnitude. This study used the most recent disaggregation data available from the 2018 NSHM of the CONUS and 2021 NSHM of HI (Petersen et al., 2019, 2022).

There are several limitations to the methodology used in this study. First, the relationship between the spectral period that the modal magnitude is being determined and T_L is

unknown and has not been investigated. With no recorded ground motions of $M_w \geq 6.5$ available but a known history of large-magnitude earthquakes in the New Madrid seismic zone (NMSZ), the expressions developed by Brune (1970) were used for even large-magnitude earthquakes. An alternative methodology for determining T_L that could be investigated in future studies is estimating T_L using displacement response spectra developed from NGA-West2 GMPEs or from NGA-East GMMs. Additionally, T_L was only calculated for the CONUS and Hawaii. Once disaggregation data and estimates of seismological parameters are readily available in Alaska and US territories, T_L needs to be investigated and potentially modified in those areas as well.

Acknowledgments

The authors would like to thank Arash Zandieh for providing reviews and recommendations. We would also like to thank Ali Farhadi for his assistance with the Selenium web driver function. Finally, we would like to thank the reviewers for their thoughtful comments that greatly improved this document.


Declaration of conflicting interests

The author(s) declared no potential conflicts of interest with respect to the research, authorship, and/or publication of this article.

Funding

The author(s) received no financial support for the research, authorship, and/or publication of this article.

ORCID iD

Shahram Pezeshk  <https://orcid.org/0000-0002-4367-1184>

Data and resources

The ground motion characterization (GMC) tool for the CEUS GMMs is available at <https://www.risksciences.ucla.edu/nhr3/ngaeast-gmtools> from Goulet et al. (2018). The USGS Disaggregation Web Tool is available at <https://earthquake.usgs.gov/nshmp/> from USGS (2022). The longitude coordinates, latitude coordinates, and final T_L values calculated in this study are available at https://github.com/cmmore11/TL_US_Estimation_2022.

References

- Abrahamson NA, Silva WJ and Kamai R (2014) Summary of the ASK14 ground motion relation for active crustal regions. *Earthquake Spectra* 30: 1025–1055.
- American Society of Civil Engineers (ASCE) (2005) *Minimum Design Loads for Buildings and Other Structures*, ASCE/SEI 7–05. Reston, VA: ASCE.
- American Society of Civil Engineers (ASCE) (2016) *Minimum Design Loads for Buildings and Other Structures*, ASCE/SEI 7–16. Reston, VA: ASCE.
- American Society of Civil Engineers (ASCE) (2022) *Minimum Design Loads for Buildings and Other Structures*, ASCE/SEI 7–22. Reston, VA: ASCE.
- Atkinson GM (1993) Earthquake source spectra in eastern North America. *Bulletin of the Seismological Society of America* 83(6): 1778–1798.
- Atkinson GM and Silva WJ (2000) Stochastic modeling of California ground motions. *Bulletin of the Seismological Society of America* 90(2): 255–274.

- Bazzurro P and Cornell CA (1999) Disaggregation of seismic hazard. *Bulletin of the Seismological Society of America* 89(2): 501–520.
- Bommer JJ, Elnashai AS and Weir AG (2000) Compatible acceleration and displacement spectra for seismic design codes. In: *Proceedings of 12th world conference on earthquake engineering*, Upper Hutt, New Zealand, 30 January–4 February.
- Boore DM (2003) Prediction of ground motion using the stochastic method. *Pure Applied Geophysics* 160: 635–676.
- Boore DM (2012) Updated determination of stress parameters for nine well-recorded earthquakes in Eastern North America. *Seismological Research Letters* 83(1): 190–199.
- Boore DM, Stewart JP, Seyhan E and Atkinson GM (2014) NGA-West2 equations for predicting PGA, PGV, and 5% damped PSA for shallow crustal earthquakes. *Earthquake Spectra* 30: 1057–1085.
- Bozorgnia Y, Abrahamson NA, Atik LA, Ancheta TD, Atkinson GM, Baker JW, Baltay A, Boore DM, Campbell KW, Chiou BSJ, Darragh R, Day S, Donahue J, Graves RW, Gregor N, Hanks T, Idriss IM, Kamai R, Kishida T, Kottke A, Mahin SA, Rezaeian S, Rowshandel B, Seyhan E, Shahi S, Shantz T, Silva W, Spudich P, Stewart JP, Watson-Lamprey J, Wooddell K and Youngs R (2014) NGA-West2 research project. *Earthquake Spectra* 30: 973–987.
- Brune JN (1970) Tectonic stress and the spectra of seismic shear waves from earthquakes. *Journal of Geophysics Research* 75(26): 4997–5009.
- Building Seismic Safety Council (BSSC) (2004a) *NEHRP Recommended Provisions for Seismic Regulations for New Buildings and Other Structures Provisions*. Washington, DC: BSSC.
- Building Seismic Safety Council (BSSC) (2004b) *NEHRP Recommended Provisions for Seismic Regulations for New Buildings and Other Structures Commentary*. Washington, DC: BSSC.
- Building Seismic Safety Council (BSSC) (2015) *NEHRP Recommended Provisions for Seismic Regulations for New Buildings and Other Structures Provisions and Commentary*. Washington, DC: BSSC.
- Building Seismic Safety Council (BSSC) (2020) *NEHRP Recommended Provisions for Seismic Regulations for New Buildings and Other Structures Provisions and Commentary*. Washington, DC: BSSC.
- Campbell KW and Bozorgnia Y (2014) NGA-West2 ground motion model for the average horizontal components of PGA, PGV, and 5% damped linear acceleration response spectra. *Earthquake Spectra* 30: 1087–1115.
- Chiou BS-J and Youngs RR (2014) Update of the Chiou and Youngs NGA model for the average horizontal component of peak ground motion and response spectra. *Earthquake Spectra* 30: 1117–1153.
- Crouse CB, Leyendecker EV, Somerville PG, Power M and Silva WJ (2006) Development of seismic ground-motion criteria for the ASCE 7 standard. In: *Proceedings of 8th US national conference on earthquake engineering*, Oakland, CA, 18–22 April.
- Fauzi UJ, Fauzi A, Irsyam M, Toha FX and Hendriyawan H (2011) Proposed long-period transition map for new Indonesia earthquake resistant building code based on Indonesia seismic hazard map 2010. In: *Proceedings of annual international conference Syiah Kuala University*, Banda Aceh, Indonesia, 29–30 November.
- Goldberg DE (1989) *Genetic Algorithms in Search, Optimization, and Machine Learning*. New York: Addison-Wesley Publishing Company, Inc.
- Goulet CA, Bozorgnia Y, Abrahamson NA, Kuehn N, Atik LA, Youngs R and Graves R (2018a) Central and Eastern North America ground—motion characterization—NGA-East final report. Technical report, Pacific Earthquake Engineering Research Center (PEER), Berkeley, CA, August.
- Goulet CA, Bozorgnia Y, Abrahamson NA, Kuehn N, Atik LA, Youngs R and Graves R (2018b) NGA-east ground motion characterization tool (GMC) (Software). Accessed 23 August 2022. Available at: <https://www.risksciences.ucla.edu/nhr3/ngaeast-gmtools>
- Goulet CA, Bozorgnia Y and Abrahamson NA (2015) PEER NGA-East: Median ground motion models for the central and eastern North America region. Technical report, Pacific Earthquake Engineering Research Center (PEER), Berkeley, CA, April.

- Gregor NJ, Silva WJ, Wong IG and Youngs R (2002) Ground motion attenuation relationship for Cascadia subduction zone megathrust earthquakes based on a stochastic finite fault model. *Bulletin of the Seismological Society of America* 92(5): 1923–1932.
- Hanks TC and Kanamori H (1979) A moment magnitude scale. *Journal of Geophysical Research* 84(5): 2348–2350.
- Harmsen S (2001) Mean and modal epsilon in the deaggregation of probabilistic ground motion. *Bulletin of the Seismological Society of America* 91: 1537–1552.
- Hashash YMA, Okan I, Harmon JA, Parker GA, Stewart JP, Rathje EM, Campbell KC and Silva WJ (2020) Nonlinear site amplification model for ergodic seismic hazard analysis in Central and Eastern North America. *Earthquake Spectra* 36(1): 69–86.
- Idriss IM (2014) An NGA-West2 empirical model for estimating the horizontal spectral values generated by shallow crustal earthquakes. *Earthquake Spectra* 30: 1155–1177.
- Ji C and Archuleta RJ (2021) A source physics interpretation of non-self-similar double-corner frequency source spectral model JA19_2S. *Bulletin of the Seismological Society of America* 111(2): 737–761.
- Kircher & Associates (2015) *Investigation of an Identified Shortcoming in the Seismic Design Procedures of ASCE 7-10 and Development of Recommended Improvements for ASCE 7-16*. Washington, DC: Kircher & Associates.
- Kircher CA, Rezaeian S and Luco N (2019) Proposed multi-period response spectra and ground motion requirements of the 2020 NEHRP recommended provisions and ASCE 7-22. In: *Proceedings of SEAOC convention 2019*, Squaw Creek, CA, 28–31 August.
- Koza JR (1992) *Genetic Programming: On the Programming of Computers by Means of Natural Selection*. Cambridge, MA: Massachusetts Institute of Technology Press.
- Li B, Xie WC and Pandey MD (2016) Newmark design spectra considering earthquake magnitudes and site categories. *Earthquake Engineering and Engineering Vibration* 15(1): 519–535.
- McVerry GH, Houtte CV, Kaiser A, Holden C, Fry B and Gerstenberger M (2017) The transition period TL in the recommended spectra of the draft New Zealand seismic isolation guidelines. In: *Proceedings of New Zealand society for earthquake engineering conference*, Wellington, New Zealand, 27–29 April.
- Mallhotra PK (2006) Smooth spectra of horizontal and vertical ground motions. *Bulletin of the Seismological Society of America* 96(2): 506–518.
- Newmark NM and Hall WJ (1973) *Procedures and Criteria for Earthquake-resistant Design, Building Practices for Disaster Mitigation (Building Sciences Series 46)*. Washington, DC: US Department of Commerce.
- Petersen MD, Shumway AM, Powers PM, Moschetti MP, Llenos AL, Michael AJ, Mueller CS, Frankel AD, Rezaeian S, Rukstales KS, McNamara DE, Okubo P, Zeng Y, Jaiswal KS, Ahdi SK, Altekruze JM and Shiro B (2022) 2021 U.S. National Seismic Hazard Model (NSHM) for the state of Hawaii. *Earthquake Spectra* 38: 865–916.
- Petersen MD, Shumway AM, Powers PM, Mueller CS, Moschetti MP, Frankel AD, Rezaeian S, McNamara DE, Luco N, Boyd OS, Rukstales KS, Jaiswal KS, Thompson EM, Hoover SM, Clayton BS, Field EH and Zeng Y (2019) 2018 update of the U.S. national seismic hazard model: Overview of model and implications. *Earthquake Spectra* 36(1): 5–41.
- Silva WJ, Abrahamson NA, Toro G and Constantino C (1997) Description and validation of the stochastic ground motion model. Unpublished report prepared for the Brookhaven National Laboratory, Brookhaven National Laboratory, Upton, NY, November.
- Stewart JP, Parker GA, Atkinson GM, Boore DM, Hashash YMA and Silva WJ (2020) Ergodic site amplification model for central and eastern North America. *Earthquake Spectra* 36(1): 42–68.
- United States Geological Survey (USGS) (2022) beta: NSHM hazard tool, software. Accessed 25 July 2022. Available at: <https://earthquake.usgs.gov/nshmp/>
- United States Nuclear Regulatory Committee (USNRC) (1973) *Regulatory Guide 1.60, Design Response Spectra for Seismic Design of Nuclear Power Plants*. Washington, DC: United States Nuclear Regulatory Committee (USNRC).

- Wong I, Darragh R, Smith S, Wu Q, Silva WJ and Kishida T (2021) Ground motion models for shallow crustal and deep earthquakes in Hawaii and analyses of the 2018 M 6.9 Kalapena sequence. *Earthquake Spectra* 38(1): 579–614.
- Zandieh A, Pezeshk S and Campbell KW (2018) An equivalent point-source stochastic simulation of the NGA-West2 ground-motion prediction equations. *Bulletin of the Seismological Society of America* 108(2): 815–835.